# Magnetic Properties of Block-Copolymer Fabricated Cobalt Nanodots and Nanowires at Elevated Temperatures

by

Juan J. Hernandez

SUBMITTED TO THE DEPARTMENT OF MATERIALS SCIENCE AND ENGINEERING IN PARTIAL FULFILLMENT OF THE REQUIREMENTS FOR THE DEGREE OF

Bachelor of Science

at the

Massachusetts Institute of Technology

May 2015



Signature of Author……
Department of Materials Science and Engineering
May 1, 2015

Certified by……
Caroline A. Ross
Toyota Professor of Materials Science and Engineering
Thesis Supervisor

Accepted by……...
Geoffrey S.D. Beach
Associate Professor of Materials Science and Engineering
Chair of the Undergraduate Committee

## Abstract

Patterned media on the nanometer scale are useful for electrical, optic, and magnetic applications such as memory storage. Using block copolymer fabrication methods, 60nm diameter cobalt nanodots and 37nm wide cobalt nanowires were created, both with heights of 20nm. To characterize the reliability of the nanodots, magnetic hysteresis loops of three samples, Co5 Co7 and Co9, were taken at elevated temperatures up to 350℃. Comparing room temperature magnetization to the ideal magnetization, percent of surface covered in nanodots was calculated to be 88%, 50%, and 60% respectively for each sample. The trends of magnetization per square centimeter and coercivity with temperature both suggest 2 mechanisms are involved in decreasing the magnetic properties of the nanodots; oxidation occurring below 200℃ and microstructure rearrangement occurring above 200℃. The depth of oxide growth on the nanodots was calculated to be 2nm deep on the surface of the nanodots when below 200℃ and no more than 10nm deep when above 200℃. Activation volume calculations could not be accurately calculated, suggesting an activation volume $10^{-7}$ times the volume of one nanodots. To characterize magnetic features present in the nanowires from block copolymer fabrication, magnetic force microscopy images were taken of direct and alternating demagnetized samples for a qualitative analysis. Counting magnetic features showed direct demagnetized samples had more 50% domain walls, with the domain walls mainly located on junctions and curves. Alternating demagnetized samples had fewer domain walls and these were predominantly located in straight lines.

## Acknowledgements

This research could not have been possible without the dedication and help from many others. I would like to thank Kun-hua Tu who helped guide me through the experimental process and the last-minute mishaps. I also thank Professor Ross, whose invaluable insight helped me pull much understanding from the hysteresis curves. Lastly, thanks to my fellow thesis peers Annia Pan, Alice Chen, Cecilio Aponte, Dohyun Bae, and Jenny Lu who encouraged me throughout the thesis process all along.

## Table of Contents


**List of Figures** ..... 5

**List of Tables** ..... 7

**Introduction** ..... 8

**Theoretical Background** ..... 10

- **Hysteresis Loops** ..... 10
- **Activation Volume** ..... 12
- **Magnetic Force Microscopy** ..... 12
- **Domain Walls** ..... 13
- **Demagnetization** ..... 15

**Fabrication** ..... 16

**VSM Tests of Cobalt Nanodots** ..... 19

- **Testing Methods** ..... 19
- **VSM Data** ..... 20
- **Percent Sample Coverage** ..... 28
- **Depth of Oxidation** ..... 30
- **Calculating Activation Volume** ..... 33

**Magnetic Features from DC and AC Demagnetization** ..... 35

- **Labeling Method** ..... 35
- **Demagnetization Magnetic Features** ..... 36

**Conclusion** ..... 38

**Works Cited** ..... 41

## List of Figures

Figure 1. Schematic of layers formed after applying BCP on substrate ..... 8

Figure 2. Typical hysteresis curve ..... 10

Figure 3. Typical MFM image (right) of cobalt nanowire sample along with its AFM image (left) ..... 13

Figure 4. Field lines for a 180° domain wall ..... 14

Figure 5. Alternating current demagnetization method ..... 15

Figure 6. Schematic of pattern transfer using block co-polymer self-assembly and ion-beam etching ..... 17

Figure 7. Top and cross-section SEM images of nanodots during fabrication. ..... 17

Figure 8. SEM image of the Co5 sample surface ..... 18

Figure 9. VSM heating setup for samples ..... 20

Figure 10. Hysteresis loops of Co7 sample tested at elevated temperatures ..... 21

Figure 11. Hysteresis loops of Co9 sample tested at elevated temperatures ..... 22

Figure 12. Hysteresis loops of Co12 sample tested at elevated temperatures ..... 22

Figure 13. Magnetization per square centimeter as a function of temperature Co5, Co7, and Co9 samples ..... 25

Figure 14. Coercivity as a function of sample temperature for Co5, Co7, and Co9 samples ..... 26

Figure 15. SEM image of cobalt nanodots at room temperature, post 350 C heating ..... 27

Figure 16. Oxide growth prediction on cobalt nanodots surface ..... 30

Figure 17. Oxide growth as a function of temperature for Co5. ..... 32

Figure 18. Typical result from labeling a cobalt nanowire sample with relevant physical and magnetic features ..... 36

Figure 19. Common magnetic features seen on DC and AC demagnetized samples..... 37

## List of Tables

Table 1. VSM test parameters. ..... 19

Table 2. List of temperature tests conducted ..... 20

Table 3. Magnetization and coercivity values for hysteresis loops ..... 24

Table 4. Calculating percent of surface covered from two methods ..... 29

Table 5. Activation volume calculated for Co5 and Co9 samples ..... 34

## Introduction

Current technology has been searching easy, reproducible ways to create features 100nm and smaller. When being able to pattern features on this scale, applications in electronics, photonics, optoelectronics, and magnetism emerge start as patterned media data storage [1]. One way to process these small features is through block-copolymers. These polymers are made from immiscible blocks and held together by covalent bonds. When they are mixed in the right ratios they blocks undergo micro phase separation, creating a patterned film. Specifically, with a sufficiently high enough Flory-Higgins interaction parameter $\chi$, features of around 5-100nm can be obtained [2]. Using this fabrication method cobalt nanodots and nanowires were created, and a schematic of this method is shown in **Error! Reference source not found.**.

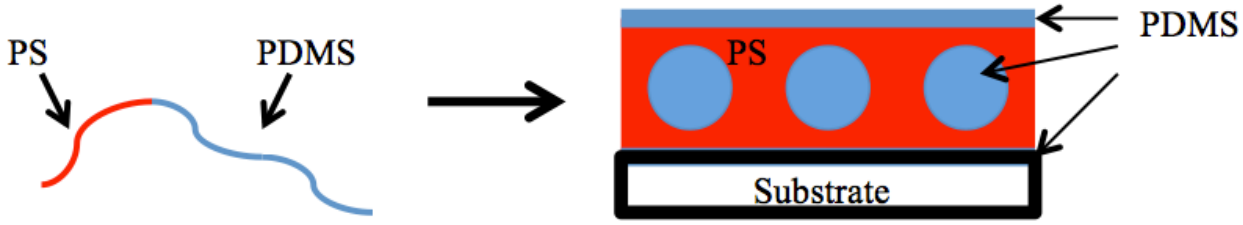


**Figure 1. Schematic of layers formed after applying BCP on substrate. Etching away top layer of PDMS and PS reveals the nanometer pattern on the surface [2].**

This study characterizes the cobalt nanodots and nanowires to further their application in the fields of electronics, photonics, optoelectronics or magnetism. The nanodots were characterized by measuring their hysteresis loops at elevated temperatures up to 350℃. This work is unique in the field in that it sought to calculate the activation volume for the nanodots. This activation volume would be useful in predicting the magnetic characteristics of the nanodots should they choose to be used in data storage technology in the future. The dimensions of the nanodots

studied were on average 60nm in diameter and 20nm in diameter. The nanowires were characterized by qualitatively analyzing their physical features, analyzing their magnetic features, and trying to find correlations between the two. Furthermore, the nanowires were qualitatively analyzed for their magnetic characteristics after demagnetization. Direct current and alternating current demagnetizations were studied and compared. This work is also unique in the field and would be useful in predicting the magnetic characteristics of the nanowires. The dimensions of the nanowires were on average 37nm in width and 20nm in height.

This thesis is organized to cover the two topics of cobalt nanodots and nanowires. First the theoretical background will cover background knowledge needed for future analysis. Then the work will cover VSM, temperature's effect on the cobalt nanodots, tests performed and their results. From these results methods to calculate the fraction of the surface covered with periodic nanodots, the level of oxidation that occurs on the samples at different temperature, and the activation volume are discussed. Then qualitative analysis of the MFM images used to characterize DC and AC demagnetized cobalt nanowires are discussed and the method used to label their physical and magnetic features. The relationship between physical features and magnetic features when conducting both direct current and alternating current demagnetization is finally discussed.

# Theoretical Background

## Hysteresis Loops

Hysteresis loops are loops taken of the relationship between the field applied to a material and the magnetization of the material itself. The applied field is H, measured in Oersteds or $Oe$ for short, and the magnetization of the material is M, measured in $emu/cm^3$. The magnetization of the material, M, can easily be converted to the magnetic flux density a material experiences, B. The conversion follows from the equation $B = \mu_o \mu_r M$, where $\mu_o$ is the magnetic permeability free space and $\mu_r$ is the relative permeability in a specific material [3]. The hysteresis graph usually provides 3 important pieces of information. They are the coercivity of the magnetic material, the magnetization, and the energy dissipated when the material switches from one magnetic orientation to another. Figure 2 shows a typical hysteresis loop.

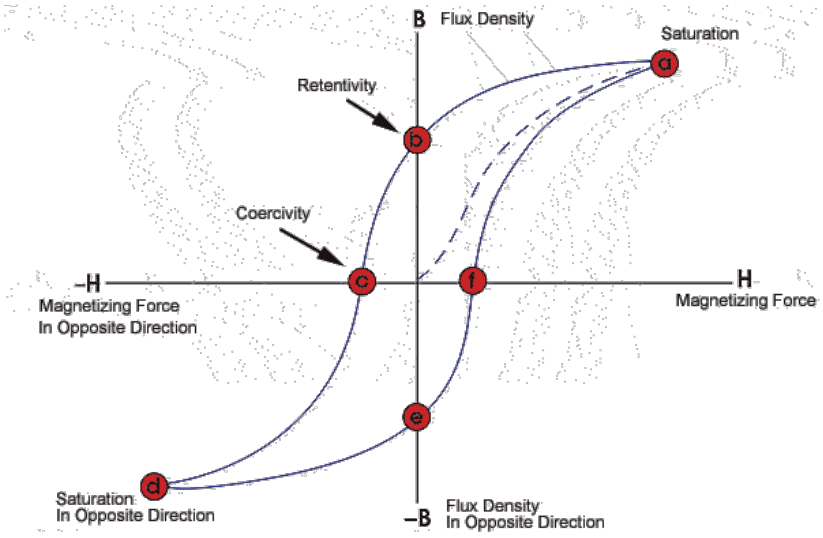


**Figure 2. Typical hysteresis curve. Notice the common parts of the curve include the coercivity, saturation magnetization, and remanence [4].**

The coercivity is known as $H_C$ and is known as the value of the field at which the magnetization reaches zero. The magnetic saturation is the largest value of M that the material reaches while the remanence is the magnetization value the material keeps even when the applied field is turned down to zero. The energy dissipated when a material switches magnetic direction is the area within the curve of the B(H) hysteresis loop. For measurements using M, the loop must be multiplied by $\mu_r$. Increasing $H_C$ for a material will result in a larger inside area and thus take more energy for the material to switch over. There are two different types of materials based on their hysteresis curves: hard magnets and soft magnets. Hard magnets have large $H_C$ and dissipate a lot of energy when it switches magnetic directions. Thus it is difficult to make hard magnets switch their directions, making them optimal for storing memory for long periods of time. Soft magnets on the other hand have small $H_C$ value and dissipate little energy when they switch over. This makes them easy to use them when trying to create alternating magnetic fields in electromagnets [3].

When magnetic materials are raised temperature, their magnetic properties begin to diminish. This is because magnetism is related to the spin of the electrons within the material; enough thermal energy in a material will overcome the exchange coupling between adjacent atoms in the solid, making the material become a paramagnet. For hysteresis loops, this means that the curve will have no area in the center [5]. The temperature at which the properties switch to those of a paramagnet is known as the Curie temperature. For pure Cobalt, the material worked with in this study, the Curie temperature has been measured to be 1121 ℃. Also at higher temperature, oxidation occurs at more rapid rates. The oxidation of Cobalt results in Cobalt Oxide, an

antiferromagnet [6]. Thus, when one is heating up Cobalt and measuring its magnetic properties, they must be aware of Cobalt Oxide formation and how this will affect their data.

## Activation Volume

Magnetic materials reverse their magnetization polarization in hysteresis loops part by part. The exact cluster of magnetic materials that reverse polarization at a time is random. The probability of reversal for a part of the material is $\propto e^{-KV^*/kT}$ [7]. The volume of magnetic material involved in reversal is termed the activation volume, $V^*$. Knowing $V^*$ is useful of this study because $V^*$ determine how many nanodots reverse at a time, which impacts the density of data storage. One starts trying to calculate $V^*$ by plotting $H_C$ as a function of temperature. The estimation for $V^*$ is based on the equation

$$H_C = H_o\left(1 - \left(\frac{k * T}{K_U * V^*}\right)\ln(A * \tau)\right).$$

$H_o$ stands for the original coercivity, $K_U$ for the magnetocrystalline anisotropy, k for the Boltzmann constant, T for the temperature the sample is at, $H_C$ for the coercivity, $V^*$ for the activation volume, $A$ for the attempt frequency, and $\tau$ for the time scale of measurement [8]. The slope of the $H_C$ versus $T$ plot is what gives an estimation for $V^*$,

$$slope = \frac{H_o * \ln(A * \tau) * k}{K_U * V^*}.$$

## Magnetic Force Microscopy

Magnetic force microscopy, or MFM, is done by hovering a magnetic tip over the surface of a sample. This tip can measures the gradient in vertical field coming out of the sample; MFM is

used to determine the magnetic stray field of a sample. This measurement is always coupled with atomic force microscopy, known as AFM, which measure topography. Together, the two measurements can be used to determine correlations between the physical features seen on the surface of a sample and the magnetic properties seen there [9]. A typical MFM diagram is shown in Figure 3.

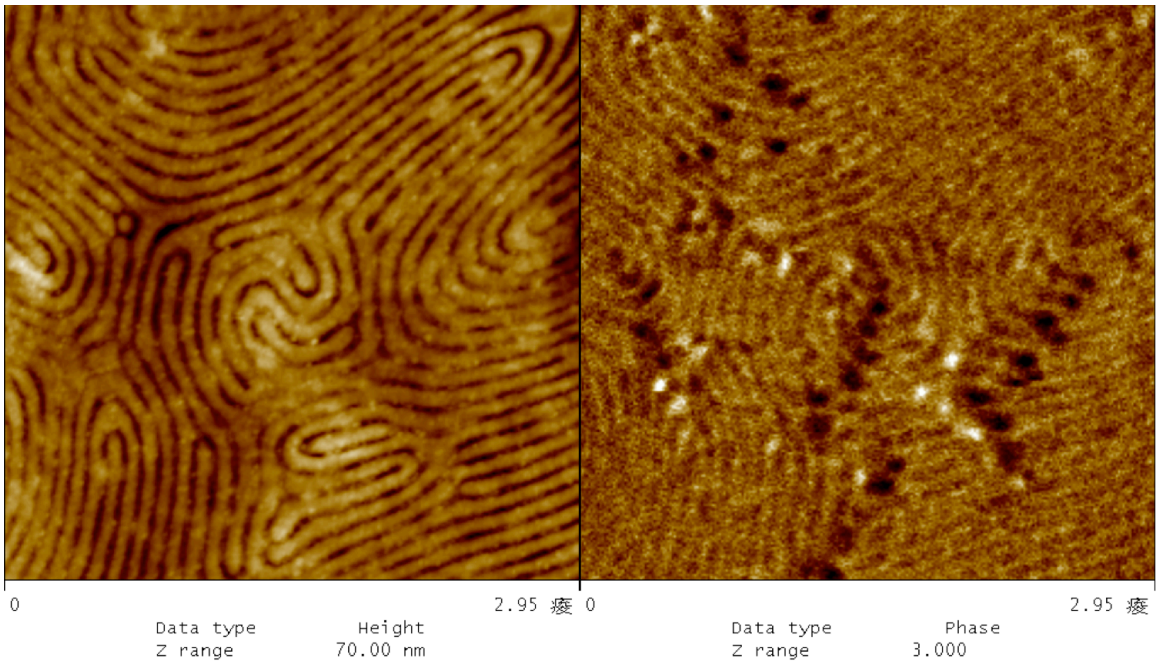


**Figure 3. Typical MFM image (right) of cobalt nanowire sample along with its AFM image (left). Both images are of cobalt nanowires and are $2.95\mu m$ wide squares.**

Through MFM experiments one learns about the perpendicular magnetic fields a sample can have. Furthermore, the tests cover an area small enough that localized magnetic fields that act like monopoles can be isolated and see how they interact with their neighbors.

## Domain Walls

Domain walls are the transitions between regions where the magnetic moment changes direction to another. Domain walls have finite thickness that slowly turns the direction of the

magnetization. There are two main factors that control the width of a domain wall. They are the magnetocrystalline anisotropy of the material and the exchange energy, $J_{ex}$. These energies are opposing; the magnetocrystalline energy favors the magnetic field to point in only certain directions and energy is lowered if the direction would switch over as narrow a distance as possible. On the other hand, the exchange energy favors the magnetic directions to be as aligned as possible and favor switching over as wide a distance as possible. Thus, the resulting domain wall is a balance of these two forces [10].

Domain walls can be viewed using magnetic force microscopy, or MFM, tests. These tests can pick up areas within a material that have a magnetic field pointing perpendicularly out of the material. Since domain walls rotate the magnetic direction of a material by having it transition through pointing outside the material, MFM can pick up the location of domain walls. Figure 4 shows this clearly.

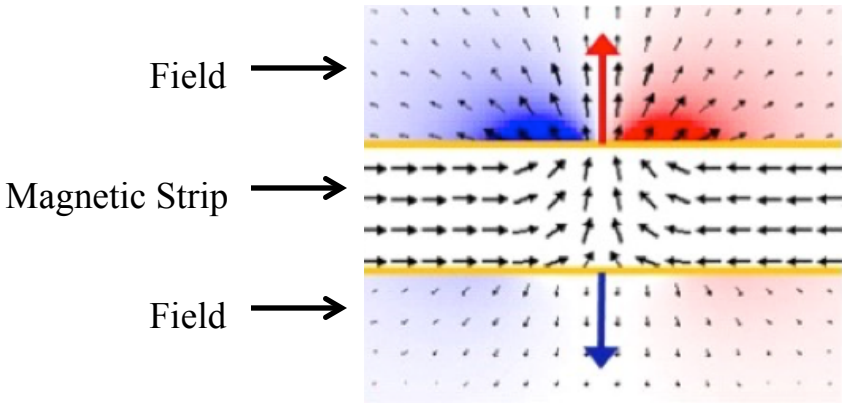


**Figure 4. Field lines for a 180° domain wall. Note that the field looks similar to a monopole in the direction of flux divergence and a dipole from the core of the wall.**

## Demagnetization

Demagnetizing a material can occur in 2 different ways. The material can undergo DC demag, which occurs when the sample directly is taken from experiencing a very high magnetic field to remanence on the loop previously shown in Figure 2. The problem with this method is that the material will still have the magnetization value of the remanence, which biases magnetic properties in favor of the applied field. The other method is alternating current demagnetization, or AC demag. This method has the sample being cycled through the extremes of the magnetization fields, while these extremes are lowered in value every time [4]. Figure 5 shows how AC demag works; DC demag works in the same way, the difference being that it stops at point Br of Figure 5. The benefits of AC demag is that the sample ends up finishing with no net magnetization. Furthermore, the magnetic features that are left within the sample have occurred because of physical features pinning down the domain walls and the dipoles.

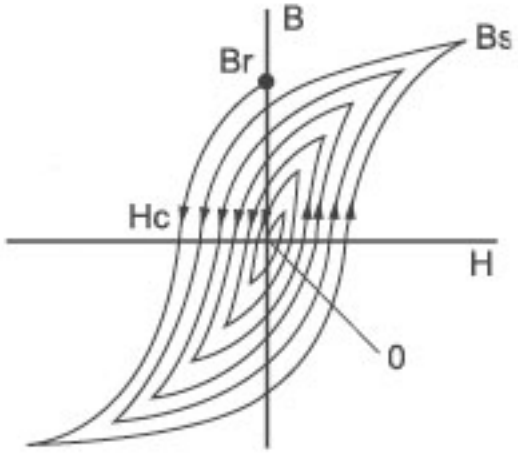


**Figure 5. Alternating current demagnetization method. Note that it demagnetizes the sample in cycles, decreasing the amplitude every time [11].**

## Fabrication

Samples were prepared by establishing an initial pattern with block co-polymers and the pattern was formed into cobalt nanodots through RIE and ion-beam etching. To begin with, silicon wafers were deposited with magnetic materials. A 5nm Ti layer, followed by a 20nm Co layer was sputtered on to the Silicon. To test the consistency of this fabrication, another silicon wafer with the same Ti-Co thin film was created and left as is to test its magnetic properties verses the patterned films. After the magnetic materials had been placed a PDMS layer was put on top and on top of that the block co-polymer was placed. After annealing and RIE one of the polymers was removed, leaving behind the desired nanometer sized patterns in the block co-polymers. RIE with $O_2$ etched this pattern in to the PMMA. Now, oxidized PMMA was left on the sample and this material is not hard enough to properly withstand ion-beam etching and accurately transfer the pattern into the cobalt. Thus, tungsten was e-beam evaporated onto the sample because it can provide a hard, stable mask. After this evaporation, the PMMA was removed via a lift-off process. The result of this step was tungsten nanodots on top of the cobalt magnetic layer. Lastly, ion-beam etching incident from a $55°$ angle milled away the remaing tungsten and imprinted the opposite pattern into the cobalt magnetic layer. The etching lasted for four minutes.

Figure 6 shows the schematic of the entire fabrication process. Figure 7 show top views and side views of the pattern transfer process. It shows that the pattern transfer method resulted in no structure breakdown. However, the tungsten nanodots and thus the cobalt nanodots did have the edges tapered off, resulting in a conical shape. This is due to the ion-beam etch; if the etch rate of the target layer is higher than tungsten then the tapered edge will be steeper and vise versa.

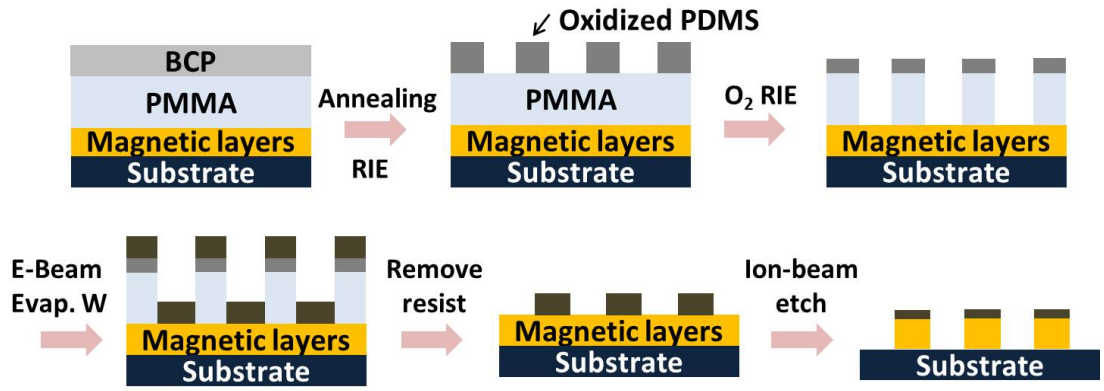


**Figure 6. Schematic of pattern transfer using block co-polymer self-assembly and ion-beam etching [12].**

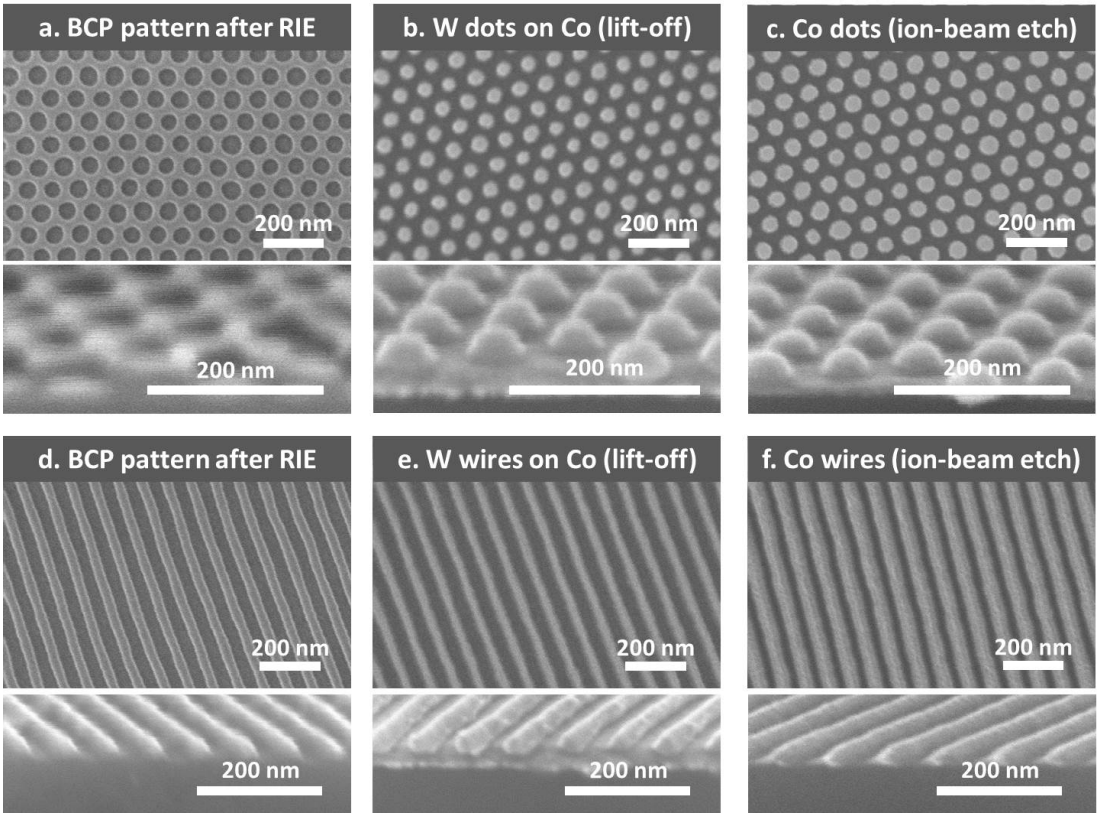


**Figure 7. Top and cross-section SEM images of nanodots during fabrication. (a), (b), and (c) show the transfer of perforated lamellae pattern while (d), (e), and (f) show the transfer of the cylinder pattern [12].**

Following the fabrication process, 3 different cobalt nanodots samples were tested. They are Co5, Co7, and Co9 and the different numbers only signify that they were created from different

batches, though all were created from the ion-beam etch process. Each sample was covered with the same cobalt nanodots, with dimensions of 60nm diameter and 20nm height. Modeling the cobalt nanodots as cylinders, the volume of a single cobalt nanodots is $5.65 * 10^{-17} cm^3$. The periodicity between cobalt nanodots was measured to be 92nm and was a close-packed arrangement [12]. The dimensions of the Co5 wafer sample are 6.40mm high and 5.71mm wide with an area of $0.365 cm^2$, the Co7 wafer sample 3.80mm high and 4.37mm wide with an area of $0.166 cm^2$, and the Co9 wafer sample 3.37mm high and 5.54mm wide with an area of $0.186 cm^2$.

Figure 8 is a representative SEM image of the surfaces of the Co5 sample. The Co7 and Co9 samples had similar surfaces. The figure shows that not the entire sample surface is covered by the nanodots. This lack of coverage reduces the overall magnetization the sample will undergo. Not all the sample surface is covered by nanodots because some of the block co-polymer had regions where the lamellae fold on each other and did not follow the typical continuity.

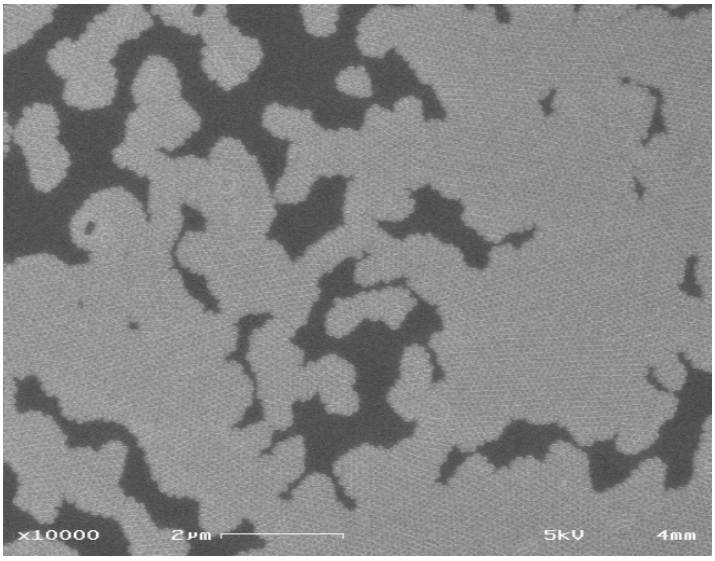


**Figure 8. SEM image of the Co5 sample surface. The light surfaces are covered in nanodots while the dark surfaces are not.**

# VSM Tests of Cobalt Nanodots

## Testing Methods

Samples were tested by running VSM tests pushing the samples from $-10{,}000\ Oe$ to $+10{,}000\ Oe$. The VSM machine was fabricated from Digital Measurement Systems and used a Model 1600 signal processor, a model 32KG gaussmeter set to a range $30\ Oe$, and Model 883A temperature controller. Samples were calibrated at the beginning of each test day. Each test took roughly 1 hour to perform. The resolution and data points taken per test are shown in Table 1.

**Table 1. VSM test parameters.**

| Field Start | Field Stop | Step Size |
|---|---|---|
| -10,000 | -3,000 | 500 |
| -3,000 | -100 | 50 |
| -100 | 100 | 10 |
| 100 | 3,000 | 50 |
| 3,000 | 10,000 | 500 |

This testing procedure was repeated for 3 different Cobalt samples. All Cobalt samples were prepared following the ion-beam etched fabrication method detailed earlier. The 3 Cobalt samples worked on were all of the same process, but had different batch numbers; they are Co5, Co7, and Co9. Each of these three samples were tested at varying elevated temperatures. To do this on the VSM, samples were mounted on silver paste. The vibrating holder was also placed within a metal-coated glass cylinder that was open at the top. The glass cylinder was heated to any temperature the user set it at, and nitrogen gas flowed into the sample to keep the sample from oxidizing. Furthermore, a solid quartz holder was used, instead of a hollow one, to be able to withstand the raised temperatures. Figure 9 shows the setup.

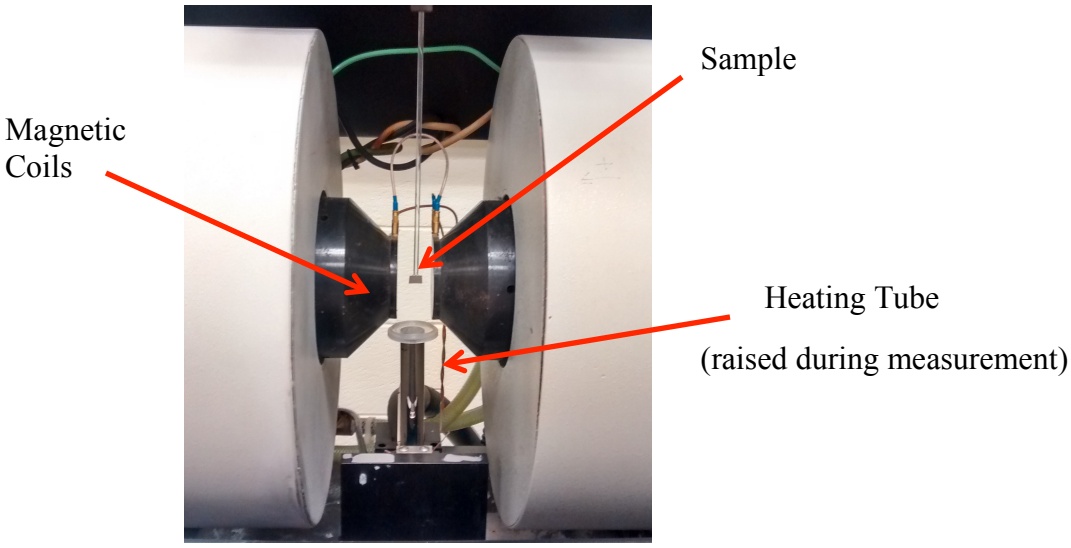


**Figure 9. VSM heating setup for samples. The heating encasing was a glass cylinder covered in metal and it was raised to cover the sample during measurement.**

Generally, samples were heated all the way up to 350°$C$ to test their thermal behavior without irreversibly affecting the magnetic properties of the Cobalt. Several tests were conducted at room temperature after the sample was raised to 350°$C$ to verify that the sample was not changed, and these samples are referred to as 25°$C$ (post350) samples. The entire list of tests is listed in Table 2.

**Table 2. List of temperature tests conducted. Co5, Co7, and Co9 samples contain nanodots of 60nm diameter and 20nm height produced by ion-beam etching.**

| Sample | Temperature Tests (°C) | Sample Area ($cm^2$) |
|---|---|---|
| Co5 | 25, 50, 100, 150, 200, 250, 300, 350, 25 (post350) | 0.365 |
| Co7 | 25, 350, 25 (post350) | 0.166 |
| Co9 | 25, 100, 200, 350, 25 (post350) | 0.186 |

## VSM Data

The resulting VSM data is shown in Figure 10, Figure 11, and Figure 12. The figures overlay the hysteresis curves for all the temperatures tested. The samples were tested in the order of Co7,

then Co9, and lastly Co5. As a result, the data for Co7 and Co9 are not as comprehensive as Co5. Co7 was tested to initially check if any irreversible effects took place when the sample was raised to 350℃. As Figure 10 shows, taking room temperature (25℃) measurements after heating to 350℃ did change the hysteresis curve. Thus, Co9 was tested with a little more caution to try and pinpoint where the irreversible change occurred. Co9 seemed to point to the change occurring between 200℃ and 350℃. Thus, Co5 was a detailed experiment and measured hysteresis curves at every 50℃.

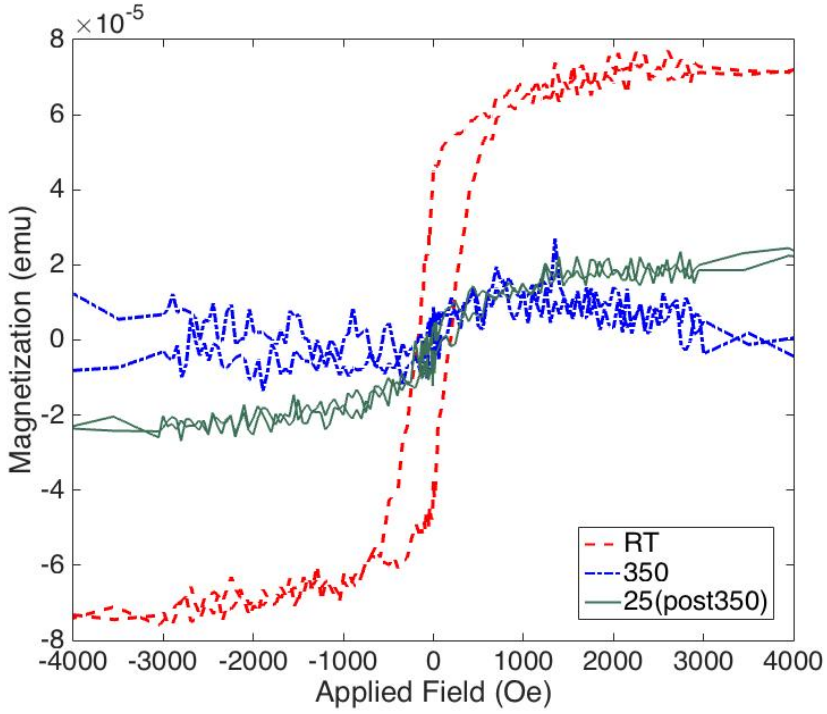


**Figure 10. Hysteresis loops of Co7 sample tested at elevated temperatures. Sample had area of $0.166cm^2$ and was tested at 25 C, 350 C, and then back at 25 C to measure irreversible change.**

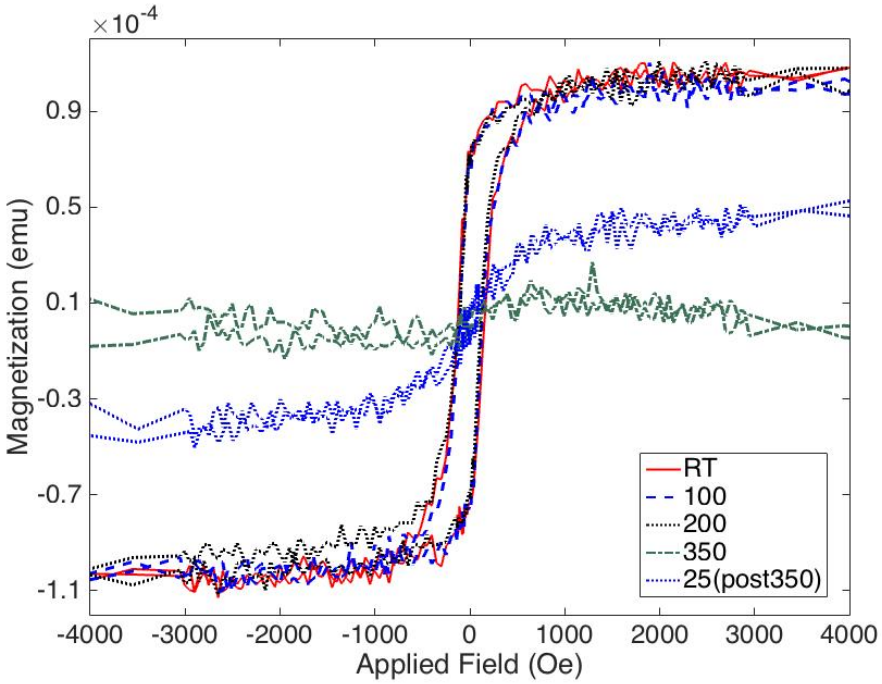


**Figure 11. Hysteresis loops of Co9 sample tested at elevated temperatures. Sample had area of $0.186cm^2$ and was tested at 25 C, 100 C, 200 C, 350 C, and then back at 25 C to measure irreversible change.**

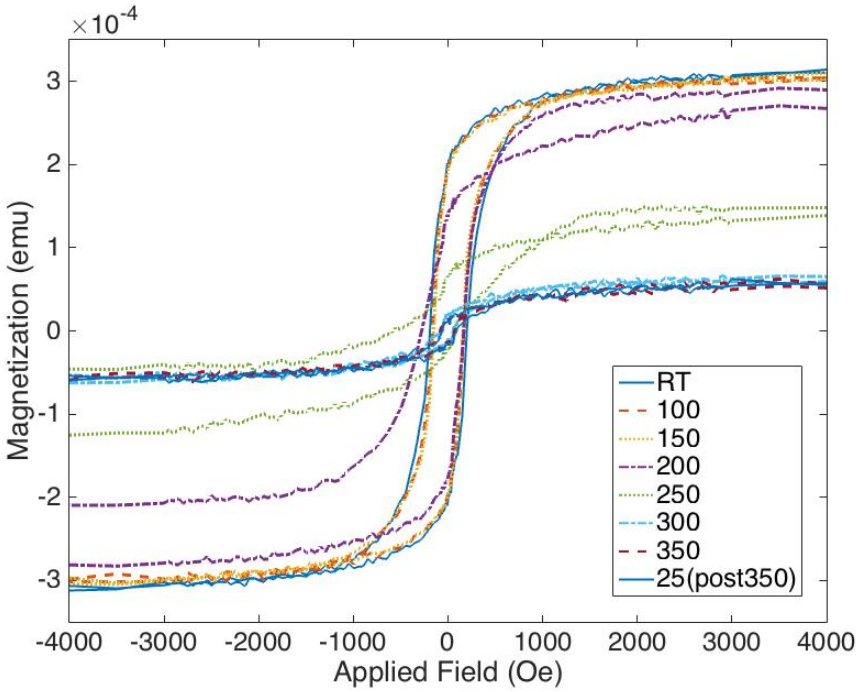


**Figure 12. Hysteresis loops of Co12 sample tested at elevated temperatures. Sample had area of $0.365cm^2$ and was tested at 25 C, 100 C, 150 C, 200 C, 250 C, 300 C, 350 C, and then back at 25 C to measure irreversible change.**

Figure 10, Figure 11, and Figure 12 show that there seem to be two different mechanisms for how the cobalt nanodots behave under high temperatures. The first mechanism appears to simply diminish the value of coercivity and saturation magnetization. It could be possible that this occurred due to some level of oxidation happening on the surface of the samples. Oxygen flow into the system would not have been impossible because the top of the heating tube was not covered, so oxygen could have flowed in. The behavior of the samples in this first mechanism occurs until roughly about 200℃ in Co9 and some point between 150℃ and 200℃ for Co5. It is uncertain whether the point at which this behavior stops working is due to a specific temperature being reached, or simply to enough heat being input into the system over time to cause some sort of change in the nanodots' microstructure. Either way, all samples had this change occur below 350℃, and Co9 and Co5 point towards the transition occurring around 200℃. After the switch occurs in the sample's coercivity and saturation magnetization drop dramatically and never go back to their original state, even after cooling. The sample seems to behave much more paramagnetically, and the background subtraction algorithm of the VSM machine had a difficult time accurately subtracting background noise because it could not distinguish the paramagnetic behavior of the sample holder from the sample itself. This is clearly seen in Figure 10 and Figure 11 where the slope of the 350℃ samples were calculated to be negative when they should have been flat. A summary of all the samples magnetic saturation and coercivity values are shown in Table 3. Error for the $M_S$, $M$, and $H_C$ values were found by finding the standard deviation of 4 different room temperature tests of the Co9 samples. This resulted in a $M_S$ error of $\pm 15\ \mu emu$ and $H_C$ error of $\pm 7.5\ Oe$. However, because $M$ is dependent on the size of each of the cobalt sample, the error for $M$ varied per sample. For Co5 error was $\pm 0.04 memu$, for Co7 $\pm 0.09 memu$, and for Co9 $\pm 0.08 memu$.

**Table 3. Magnetization and coercivity values for hysteresis loops.**

| Sample | $M_S$ $(\mu emu)$ $\pm 15\ \mu emu$ | $M$ $(memu/cm^2)$ $\pm 0.04 memu$ Co5 $\pm 0.09 memu$ Co7 $\pm 0.08\ memu$ Co9 | $H_C$ $(Oe)$ $\pm 7.5\ Oe$ |
|---|---|---|---|
| Co5 25 | 310 | 0.85 | 193 |
| Co5 100 | 303 | 0.83 | 163 |
| Co5 150 | 303 | 0.83 | 154 |
| Co5 200 | 275 | 0.75 | 207 |
| Co5 250 | 145 | 0.40 | 147 |
| Co5 300 | 60 | 0.16 | 54 |
| Co5 350 | 55 | 0.15 | 72 |
| Co5 25(post350) | 55 | 0.15 | 70 |
| Co7 25 | 80 | 0.48 | 149 |
| Co7 350 | 30 | 0.18 | 93 |
| Co7 25(post350) | 22.5 | 0.14 | 38 |
| Co9 25 | 110 | 0.59 | 134 |
| Co9 100 | 100 | 0.54 | 113 |
| Co9 200 | 105 | 0.56 | 109 |
| Co9 350 | 10 | 0.05 | 74 |
| Co9 25(post350) | 55 | 0.30 | 58 |

Plotting the magnetization per square centimeter versus temperature generates Figure 13 while plotting the coercivity versus of the sample versus temperatures generates Figure 14. Both figures show a general trend toward decreasing coercivity as temperature is raised. The coercivity data for Co5 at 200℃ and 250℃ must be taken with caution. Looking back at Figure 12, one can see that the tests at 200℃ and 250℃ had odd hysteresis structures, thus measuring their coercivity values was very challenging. The average coercivity for Co5 at 200℃ and 250℃ is showed in Figure 14, but their ranges off of the average were 40 $Oe$ and 61 $Oe$ respectively, which are much larger than the typical ranges of no more than 5 $Oe$. Aside from the downward slope, Figure 14 does not comment well on the theory of 2 different mechanisms. If the theory did hold, then one would anticipate that from the temperatures of 25℃ to 200℃ coercivity would decrease with one slope, and from 200℃ to 350℃ the coercivity would decrease with a steeper slope.

However, this exact pattern is shown in Figure 13, which shows a pretty clear change in the Co5 and Co9 results around 200℃.

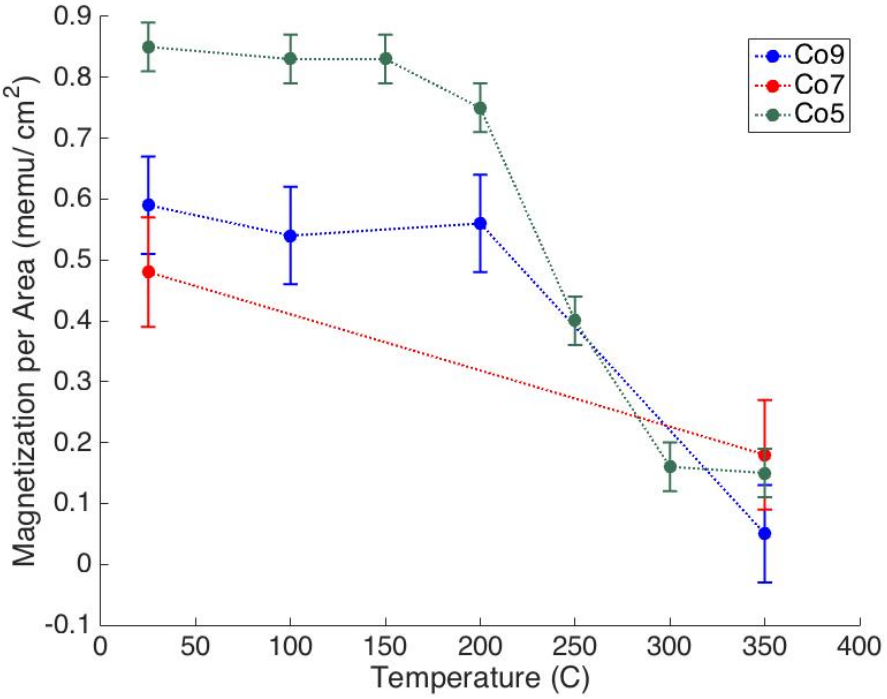


**Figure 13. Magnetization per square centimeter as a function of temperature Co5, Co7, and Co9 samples. Error was $\pm 0.04$ for Co5, $\pm 0.08$ for Co7, and $\pm 0.09 memu/cm^2$ for Co9.**

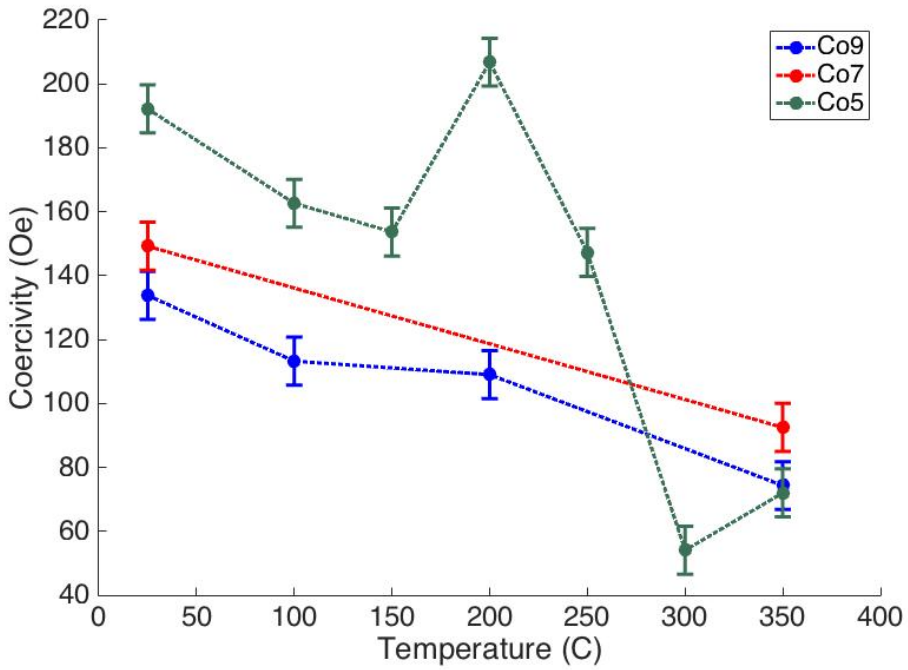


**Figure 14. Coercivity as a function of sample temperature for Co5, Co7, and Co9 samples. Error was $\pm 7.5\ Oe$ for all samples.**

To investigate the theory of two different mechanisms affecting the cobalt nanodots SEM images were taken of samples after they had been raised to 350℃. These samples were not the Co5, Co7, nor Co9 but other samples that were prepared in with the exact same fabrication methods. The results of the SEM are shown in Figure 15.

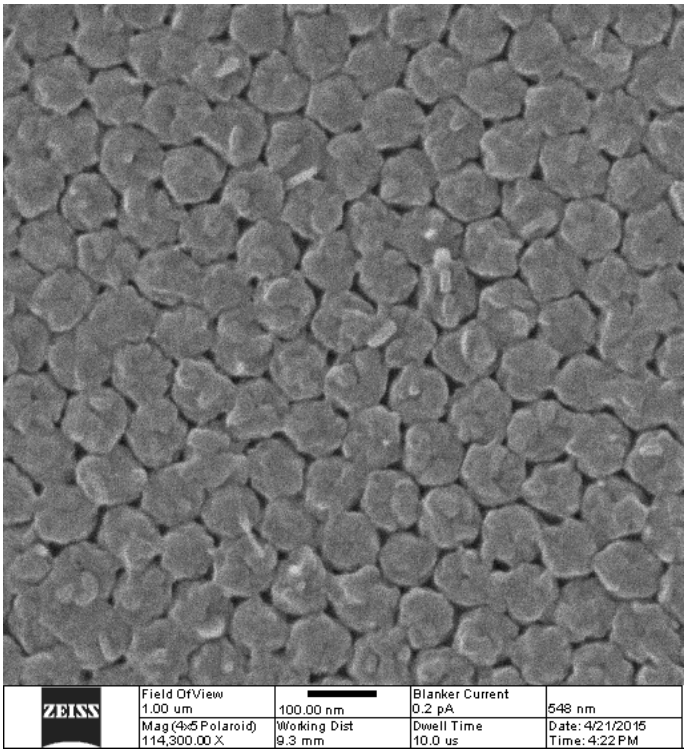


**Figure 15. SEM image of cobalt nanodots at room temperature, post 350 C heating. The scale bar shows the length of $100nm$.**

Figure 15 shows that the microstructure of the nanodots has significantly changed. Image analysis of 10 nanodots showed that the average diameter of the nanodots was now 77nm with standard deviation of 6nm, which is significantly larger than the 60nm originally were after fabrication. Image analysis of 10 different nanodots for periodicity showed the average period of the nanodots to now be 89nm with a standard deviation of 6nm. This is not very different from the originally fabricated period of 92nm, considering the standard deviation. Qualitatively comparing Figure 15 to Figure 7, one sees that after being exposed to 350℃ the nanodots had far less space between each other and some even seemed to crush together and climb on top of each other. A possible reason for why this is occurring is that the annealing temperature provides the cobalt enough energy to crystallize in preferable orientations, which could leader to flatter, wider nanodots. This change in the crystal orientation could also decrease the magnetic properties of the nanodots measure in plane by the VSM.

## Percent Sample Coverage

The Co5, Co7, and Co9 sample surfaces were not completely covered by the cobalt nanodots, as was discussed in the fabrication section. However, the magnetization can be used to determine the fraction of the sample's surface that was covered with nanodots.

Two calculations were conducted to determine the fraction of sample covered in dots. The first method was comparing my hysteresis results to literature. Tu et al. carried out similar tests on cobalt nanodots, of 60nm diameter and 20nm height on silicon wafers from block-copolymer creation and ion-beam etching. His results were that his samples had a magnetization of about $0.5 * 10^{-3} \frac{emu}{cm^2}$. This was compared to a test done on completely pure cobalt with a value of $2.71 * 10^{-3} \frac{emu}{cm^2}$, and instead of the expected 36% magnetization expected, a value of $1.00 * 10^{-3} \frac{emu}{cm^2}$, because the cobalt nanodots covered 36% of the sample surface, a value of 25.8% of the pure cobalt was obtained, or $0.70 * 10^{-3} \frac{emu}{cm^2}$. The actual 25.8% magnetization meant that only about 70% of the silicon wafer's surface was correctly covered with cobalt nanodots. The 30% of the surface not covered with nanodots was probably due to lamellae and double layer regions in the initial BCP patterns. Following this same image analysis method, the Co5, Co7, and Co9 fractions of sample surface covered were determined. The samples had their magnetization, in $\frac{emu}{cm^2}$, compared with the ideal value of $1.00 * 10^{-3} \frac{emu}{cm^2}$.

The second method is a theoretical calculation, which determines the fraction of sample covered in dots by comparing the obtained saturation magnetization with the expected theoretical value. The expected theoretical value of the saturation magnetization is found from

$$M_S = \frac{\#dots}{cm^2} * area\ of\ sample * moment\ per\ dot.$$

The samples sizes were measured and listed in the fabrication section. The $\frac{\#dots}{cm^2}$ was determined from knowing that the periodicity of the dots was 92nm and they are in a close-packed arrangement, and thus was $1.18 * 10^{10}\frac{\#dots}{cm^2}$. Lastly, the moment per dot was calculated by multiplying the cobalt's saturation magnetization of $1420\ emu/cm^3$ by the total volume found in one dot, $5.67 * 10^{-17} cm^3$. The result was $8.03 * 10^{-14}\ emu/dot$. All the cobalt samples were the same except for their size and thus the final equation was of the form

$$M_S = 1.18 * 10^{10}\frac{\#dots}{cm^2} * area\ of\ sample * 8.03 * 10^{-14} emu/dot.$$

The results of the two methods of calculating the surface area perfectly covered with dots are shown in Table 4. Note that both methods yield similar answers and support the accuracy of these figures.

**Table 4. Calculating percent of surface covered from two methods.**

| Sample | Comparing $\frac{emu}{cm^2}$ $\pm 9\%$ | Theoretical $\pm 10\%$ |
|---|---|---|
| Co5 | 85% | 90% |
| Co7 | 48% | 51% |
| Co9 | 59% | 62% |

The error for both the comparing $\frac{emu}{cm^2}$ method and the theoretical method were determined from the error of $M_s$ which was $\pm 15\ \mu emu$. Considering the error, the Co7 and Co9 samples were had similar surface coverage after fabrication, being around 50%. The Co5 sample on the other hand had a better fabrication process because its surface coverage was around 85%.

## Depth of Oxidation

It was assumed that at room temperature, the cobalt nanodots did not oxidize much. However, once temperature tests occurred the irreversible changes in magnetization and coercivity point toward oxidation. Oxide layers would form on the surfaces of the nanodot that were directly in contact with the ambient air. Figure 16 offers a simple visual for how this would occur.

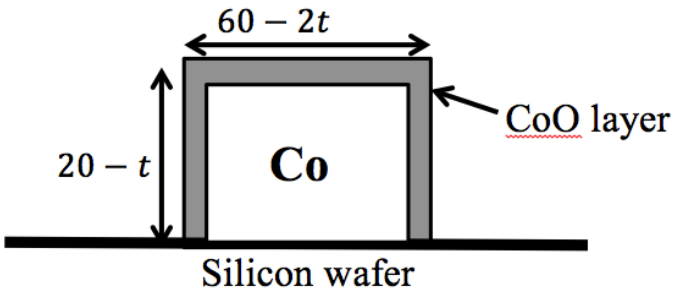


**Figure 16. Oxide growth prediction on cobalt nanodots surface. The thickness of the oxide is variable t. Notice that only the sides of the nanodot in direct contact with the air experience oxidation.**

According to the oxidation model, the new volume of magnetic material, $V_{OM}$, in a dot is

$$V_{OM} = \pi(\frac{60nm-2t}{2})^2 * (20nm - t).$$

Once a cobalt sample oxides, the cobalt oxide layer that forms on the surface is not ferromagnetic and takes away some of the magnetic properties of the sample. Thus, the resulting $M_S$ and $H_C$ will be smaller and this was supported by the decreasing trend seen in Figure 14. The decrease $M_S$ will be proportionally smaller with the oxide layer depth, so by finding the percent decrease in $M_S$ one can calculate the percent volume decrease of each cobalt nanodot and thus determine the depth of the oxide layer that formed on the nanodots. To specific method to find the oxide layer depth starts with finding the total volume of magnetic material in a sample at room temperature. The formula is

$$V_o = \frac{M_{S,o}}{1420\frac{emu}{cm^3}},$$

where $V_o$ is the volume of magnetic material at room temperature and $M_{s,o}$ is the saturation magnetization of the sample at room temperature. After finding $V_o$, the volume of magnetic material in a sample at the elevated temperature must be found. The formula is the same, the only difference is that $M_{S,T}$, or the saturation magnetization at the elevated temperature, is now used to calculate $V_T$. After this the total number of nanodots on the sample must be determined. This is found by simply dividing the total volume of magnetic material at room temperature by the volume of magnetic material per dot at room temperature,

$$n_{dots} = \frac{M_{S,o}}{1420\frac{emu}{cm^3}} / (5.65 * 10^{-17}\,\frac{cm^3}{dot}).$$

Knowing $V_o$, $V_T$, and $n_{dots}$ one can determine the change in magnetic volume that occurred per nanodot when the nanodots were raised to temperature $T$. This change in magnetic volume must have been caused by the grown of the oxidation layer. Thus, the depth of the oxidation layer is found be equaling the change in volume per nanodots to the difference in volume if a nanodots grew an oxide layer. All together, the inequality that must be solved is

$$V_{dot} - V_{OM} = \frac{V_o - V_T}{n_{dots}},$$

where $V_{OM}$ has the variable *t* for oxidation thickness inside it and this is the variable that must be solved for in the inequality. $V_{dot}$ is the volume of a cobalt nanodot and is $5.65 * 10^{-17} cm^3$, $V_{OM}$ is the volume of the oxidation model which was described above, $V_o$ is the volume of magnetic material at room temperature, $V_T$ is the volume of magnetic material at the elevated temperature, $n_{dots}$ is the number of dots needed to come up with the room temperature volume of magnetic material.

Based on the oxidation model and calculations, the relationship between oxidation depth and temperature of sample was plotted for the Co5 samples because the Co5 data had the most data available for a trend. It is shown in Figure 17.

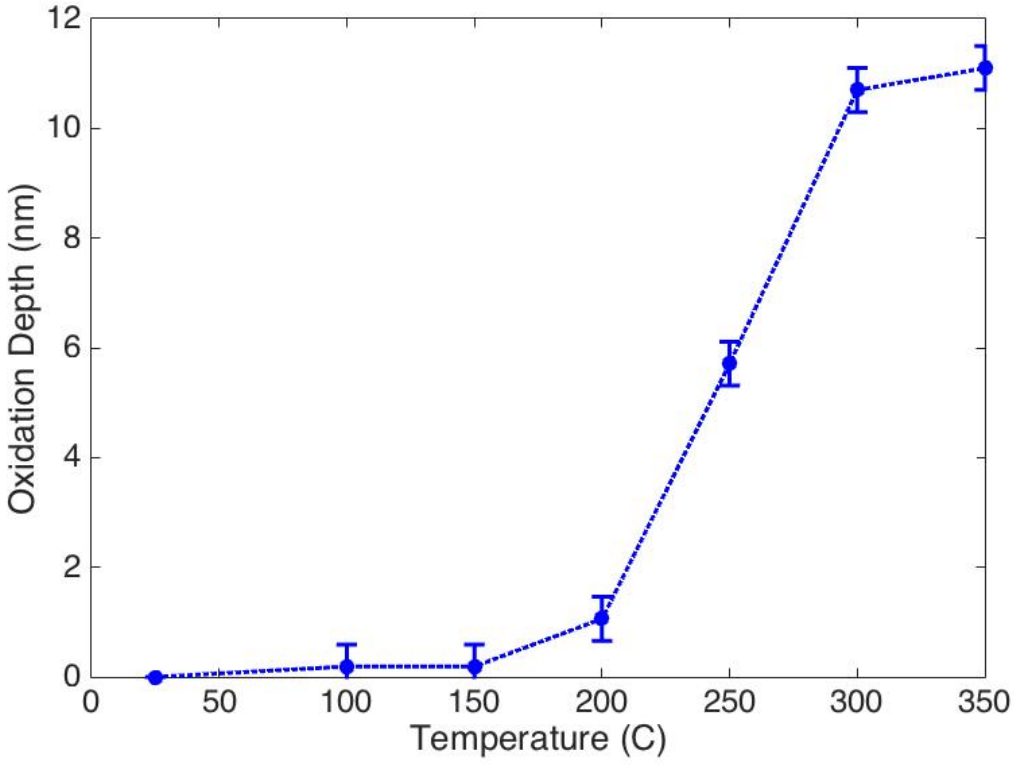


**Figure 17. Oxide growth as a function of temperature for Co5.**

It is difficult to pull too much information from Figure 17. Error for the tests was around calculated to be 0.4 $nm$ and it was calculated knowing that the $M_s$ value it is calculated from has an error of $\pm 15$ $\mu emu$. Thus, the tests that occurred from 0℃ to 200℃ all seemed to have similar oxidation depth around 2 $nm$. However, after 200℃ the mechanism by which the cobalt dots lose magnetic properties changes and oxidation depth is no longer an accurate way to explain this transition. Though whatever extent of oxidation does occur in the samples, all oxidation depth predictions point to oxidation occurring around or below 10 $nm$; all the Co5 tests had oxidation occur at or below 10 $nm$ and oxidation depth calculations performed on Co7

and Co9 post350℃ samples yielded oxidation depths of 5.3 $nm$ and 3.0 $nm$. Furthermore, for temperature tests below 200℃ the prediction point to oxidation occurring around or below 2 $nm$. Thus although the exact amount of oxidation that occurred in these samples cannot be determined, below 200℃ only about 2 $nm$ of oxidation is expected to take place and no more than 10 $nm$ of oxidation is ever expected to happen.

## Calculating Activation Volume

The activation volume, $V^*$, was found for the Co5 and Co9 samples. The Co7 sample did not have enough data taken at lower temperatures to perform the calculation. The activation volume is important to know because it tells the possible data density storage for the cobalt nanodots. As was elaborated in the theoretical background, the activation volume is found via

$$H_C = H_o\left(1 - \left(\frac{k * T}{K_U * V^*}\right)\ln(A * \tau)\right).$$

In the equation $H_o$ is equal to $\frac{2K_U}{M_s}$, k is Boltzmann constant, $M_s$ is the volumetric magnetization of pure cobalt and is 1420 $\frac{emu}{cm^3}$ or $1420 * 10^3 \frac{A}{m}$ in SI units, $K_U$ is the coefficient of magnetic anisotropy and is $4.1 * 10^5 \frac{J}{m^3}$ in pure cobalt, $A$ is the attempt frequency and is equal to $10^9 \frac{1}{s}$, $\tau$ is the time scale of measurement and is 10 $s$, and $V^*$ is the activation volume that is being solved. By plotting $H_C$ versus $T$, $V^*$ can be calculated by using the formula to find the theoretical slope. Based on the equation, $V^*$ based on the slope of the $H_C$ versus $T$ graph should be

$$V^* = \frac{2 * k * \ln(10^{10})}{M_s * slope}.$$

Note that the slope value used should be in SI units to match the units of everything else. Using this analysis, the activation volume was calculated for the Co5 and Co9 samples. Only the 25℃, 100℃, and 150℃ data points from the Co5 sample was used because after 150℃ the second mechanism of restructuring occurred in the cobalt nanodots. For the Co9 sample, only the 25℃, 100℃, and 200℃ samples were used for the same reason. The resulting activation volume are listed in Table 5. Error was calculated for slope and $V^*$ knowing that $H_C$ had an error of $\pm 7.5\ Oe$.

**Table 5. Activation volume calculated for Co5 and Co9 samples.**

| Sample | Temperatures Used | Slope $\left(\frac{Oe}{K}\right)$ $\pm 0.08$ | Activation Volume, $V^*$ $(cm^3)$ $\pm 4 * 10^{-25}$ |
|---|---|---|---|
| Co5 | 25℃, 100℃, 150℃ | $-0.3149$ | $4 * 10^{-25}$ |
| Co9 | 25℃, 100℃, 200℃ | $-0.1362$ | $1.0 * 10^{-24}$ |

Even with the large error, the results of the activation volume calculation suggest that the activation volume is far smaller than the volume of a single nanodots. In fact, the calculation suggests that the activation size is $10^{-7}$ times the volume of a single cobalt nanodot, because a single nanodot was calculated to have the volume $5.67 * 10^{-17} cm^3$. These results do not seem to be accurate. The inaccuracy most likely came from a lack of sufficient data points and furthermore only 2 samples were tested on to determine the activation volume.

## Magnetic Features from DC and AC Demagnetization

### Labeling Method

Images looked at were all ion-milled cobalt samples. Nanowires were observed. The cobalt nanowires had a thickness of 37nm and a height of 20nm. All samples were made following the same fabrication steps detailed in the fabrication section. Once these samples were prepared image analysis was done on their topography. The physical features in AFM scans were labeled and compared with magnetic features found in MFM scans of the same area, which were also labeled. It is important to note that this was a first approach, qualitative method that was not looking to make assertive conclusions.

The physical features of the nanowires that were labeled were terminations, curves, and 3-way junctions. The magnetic features labeled for nanowires white domain walls, black domain walls, junction domain walls, termination monopoles, line domain walls, and curves domain walls. To clarify, black or white dot located at a termination end was a monopole, a black or white dot located where there is no break was a 180° domain wall, and a black and white dot located next to each other was a 360° domain wall. These features were labeled to try and find any correlations between the physical features and the magnetic features. Figure 18 shows a representative image of how the samples were labeled.

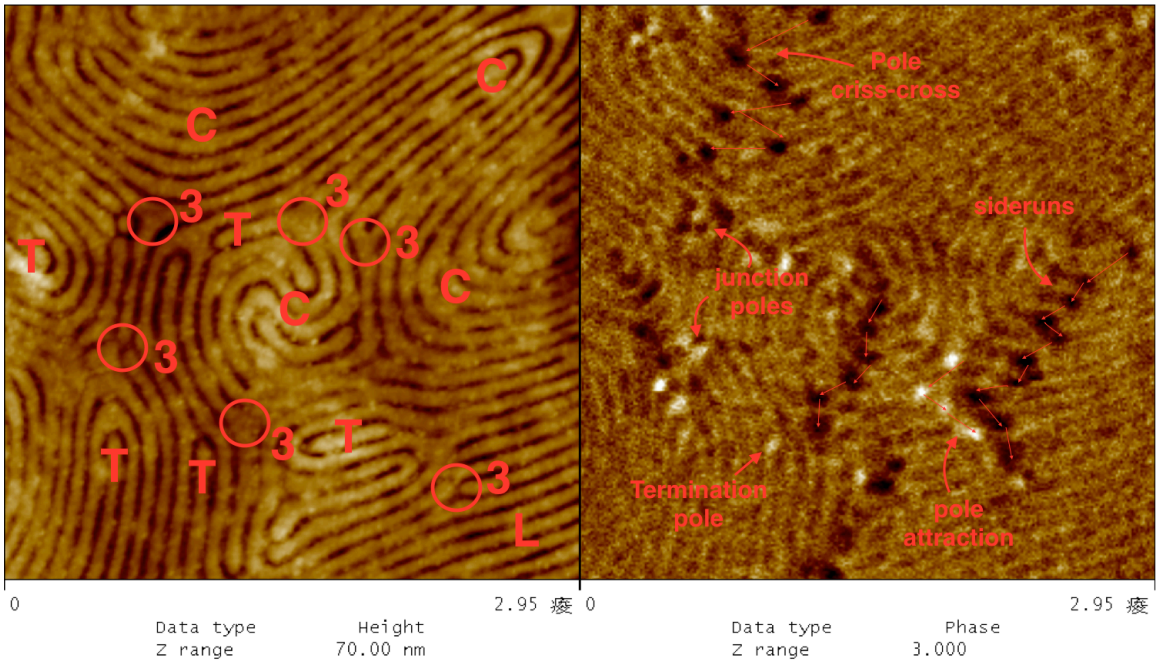


**Figure 18. Typical result from labeling a cobalt nanowire sample with relevant physical and magnetic features. Physical feature labels are a 3 stands for 3-way junction, a T for termination, and a C for curves. Both images are $2.95\mu m$ wide squares.**

## Demagnetization Magnetic Features

After labeling the magnetic features of the samples, a count was taken of them. To get the feature per square micron count, the total number of features was normalized by the area of the sample. This count was determined for four different DC demagnetization and AC demagnetization samples and the average of all these counts were determined. These averages are summarized in Figure 19.

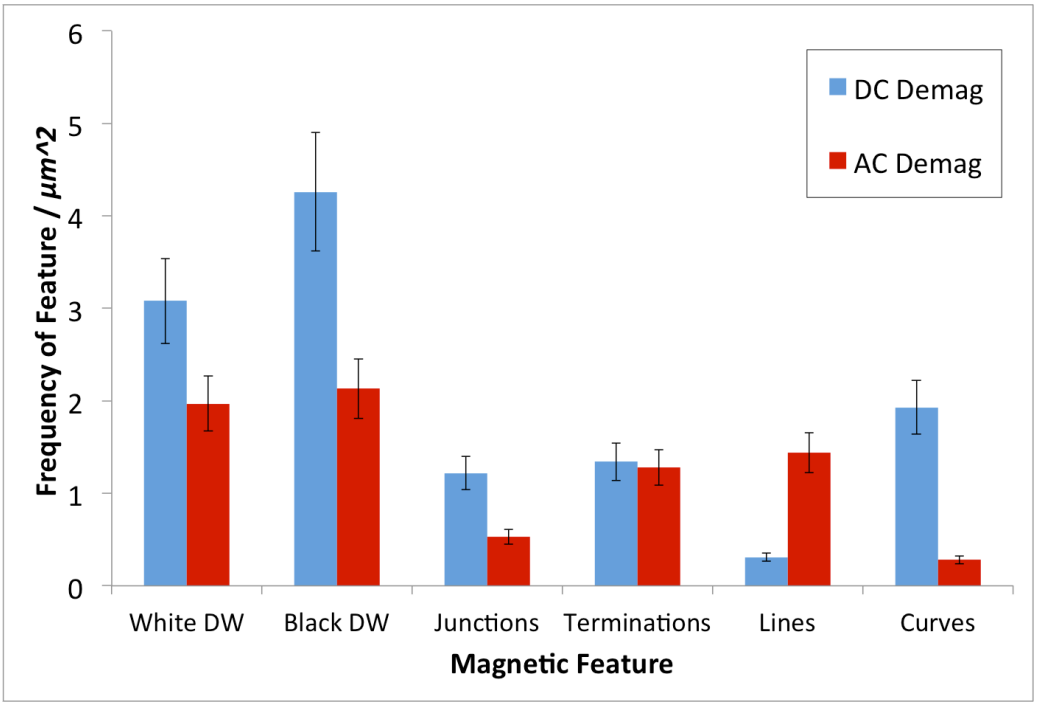


**Figure 19. Common magnetic features seen on DC and AC demagnetized samples. Frequency of the features found, per square micron, is displayed. Error is 15%.**

Figure 19 shows that DC and AC demagnetization samples differed significantly in the total number of domain walls they had, the $\mu m^2$ number of domain walls at junctions, lines, and curves. The error in calculating these features came from human errors in miscounting, leading to 15% error. The graph still shows that DC demagnetization samples overall had more white and black domain walls present in their samples. Furthermore, they were more likely to have domain walls in the junctions and the curves. AC demagnetization on the other hand had fewer white and black domain walls overall. These samples tended to have more domain walls in the lines section than in the junctions and curves. Both DC and AC demagnetization had similar numbers of domain walls appear at termination sites.

The difference in total amount of white and black domain walls can be explained by the alternating nature of AC demagnetization; in direct demagnetization the domain walls of the sample are simply moved while in alternating current demagnetization the switching field causes some domain walls to crash into and annihilate each other, leading to overall a fewer number of domain walls. The decrease in junction domain walls in the AC demagnetization samples is probably from the fact that the demagnetization samples themselves had fewer 3-way junctions to begin with. This probably biased the AC demagnetization samples to seem as though they form fewer domain walls and thus this result should be questioned. The increase in lines domain walls may have occurred because AC demagnetization keeps the domain walls moving in any direction and may eventually get pinned on a site. Since a good portion of the samples had their surface area covered with lines it makes sense that lines would now contain domain walls. These contrasts directly with the curves contained less domain walls in the AC demagnetization. In DC demagnetization, domain walls move with direction of the field and thus piled up at the curves because these were geometrically stable points. In AC demagnetization the domain walls were not pushed in any particular direction, thus it was more probable for them to end up in the lines sections, which cover a higher surface area of the sample.

## Conclusion

VSM experiments at elevated temperatures were run on the Co5, Co7, and Co9 samples and resulted in magnetization per centimeter square of $0.84 * 10^{-3} emu/cm^2$, $0.48 * 10^{-3} emu/cm^2$, and $0.56 * 10^{-3} emu/cm^2$ at room temperatures. Tests on the Co7 samples showed that raising the sample to $350℃$ irreversibly affected the sample. Co9 suggested that a critical change

in the sample occurs between 200℃ and 350℃ where the coercivity and saturation magnetization drop dramatically and do not recover to near typical values. Co5 more accurately suggested that a change occurs around 200℃. Figure 13 and Figure 14, which depict the trends of magnetization and coercivity as a function of temperature, support this theory and both show drastic change in slope around 200℃ for Co5 and Co9 samples. Furthermore, SEM image analysis of the Co5 samples post 350℃ heating in Figure 15 show the nanodots flattening out and changing microstructure.

From the hysteresis loops, the two methods of comparing saturation magnetization versus a theoretical approach both determined the fraction of sample surface covered by nanodots to be around 87%, 50%, and 60% for Co5, Co7, and Co9 which are reasonable estimates seeing the SEM images of the surface of the Co5 sample. Oxide growth explained the drop in magnetic properties below 200℃. Oxide on the nanodots sample was calculated to be around 2nm, and when above 200℃ oxide growth was calculated to be around 10nm. Activation volume calculations could not be accurately calculated and did not match theory, suggesting a activation volume for Co5 and Co9 of $4 * 10^{-25} cm^3$ and $1 * 10^{-24} cm^3$ both of which are $10^{-7}$ times the volume of one nanodots. The expected outcome would be that the activation volume is larger than the volume of a nanodots because the stray fields between dots influence each other to flip together.

Characterizing magnetic features in DC and AC demag showed DC demag had roughly 50% more domain walls than AC demag. This is most likely due to domain wall annihilation that occurs in AC demag samples from alternating the magnetic field. These domain walls were

mostly in the form of junction domain walls and curves domain walls, with curves domain walls being slightly more prevalent. These types of domain walls were 2 to 3 times more common than in AC demag samples. AC demag domain walls were mostly in the form of lines domain walls and were around 3 times as common than in DC demag samples.

Future work on cobalt nanodots should focus on finding why the cobalt nanodots changed their magnetic properties around 200℃. Specifically, SEM images should be taken of the nanodots around this temperature to visually investigate any microstructural change. Aside from this, samples with known surface coverage should be tested to verify the two surface coverage methods detailed in this thesis. The oxidation model should also be verified by taking SEM images of samples post 200℃ heating and checking for 2nm oxidation growth, and taking SEM images of samples post 350℃ heating and checking for 10nm or less oxidation growth. Lastly, more standard VSM tests should be run below 200℃ to accurately calculate the nanodots' activation volume.

## Works Cited


[1] Esterina, R. (2007). *Commercialization of Bit-Patterned Media.* Massachusetts Institute of Technology. Cambridge: MIT.

[2] Akinronbi, B. (2014). *Fabrication of Nanoscale Magnetic Domains Using Block-Copolymer Lithography.* Massachusetts Institute of Technology, Materials Science and Engineering. Cambridge: MIT.

[3] O'Handley, R. C. (2000). *Modern Magnetic Materials Principles and Applications.* Cambridge: John Wiley & Sons.

[4] The Collaboration for NDT Education. (2014, January 1). *The Hystersis Loop and Magnetic Propertires*. Retrieved April 19, 2015, from NDT Resource Center: www.nde-ed.org

[5] Friend, E. (2007). *Interaction of Stress and Magnetic Properties in Copper-Nickel-Copper Thin Films.* Massachusetts Institute of Technology, Materials Science and Engineering. Cambridge: MIT.

[6] Carlin, R. L., & Duyneveldt, A. J. (1977). *Magnetic Properties of Transition Metals.* New York: Springer-Velag.

[7] Bertotti, G. (1998). *Hystersis in Magnetism: For Physicists, Materials Scientists, and Engineers.* Boston: Academic Press.

[8] P., S. M. (1994). Time Dependence of Switching Fields in Magnetic Recording Medi. *Journal of Applied Physics , 76*, 6413.

[9] Hartmann, U. (1999). Magnetic Force Microscopy. *Annual Review of Materials Science , 29*, 53-87.

[10] Butler, R. F. (1992). *Paleomagnetism: Magnetic Domains to Geological Terranes.* Tuscon: Blackwell Scientific Publications.

[11] Nihon Denji Sokki Co. (2014, January 1). *Demagnetizer*. Retrieved April 19, 2015, from Pioneer of Magnetic Applied Industries: http://www.j-ndk.co.jp/en/

[12] Tu, K.-H., Bai, W., Liontos, G., Ntetsikas, K., Avgeropoulos, A., & Ross, C. A. *A Universal Patterning Method for Metal Nanostructures Using Block Copolymer Lithography.* Cambridge: Unpublished.

[13] Bratton, D., Yang, D., Dai, J., & Ober, C. K. (2006). Recent Progress in High Resolution Lithography. *Polymers for Advanced Technologies , 17*, 94-103.